Chapter 13: Fundamental Concepts for Guided Lamb Wave-based Structural Health Monitoring

Chapter details

Chapter DOI:

https://doi.org/10.4322/978-65-86503-71-5.c13

Chapter suggested citation / reference style:

Finzi Neto, Roberto M., et al. (2022). "Fundamental Concepts for Guided Lamb Wave-based Structural Health Monitoring". *In* Jorge, Ariosto B., et al. (Eds.) *Model-Based and Signal-Based Inverse Methods*, Vol. I, UnB, Brasilia, DF, Brazil, pp. 472–501. Book series in Discrete Models, Inverse Methods, & Uncertainty Modeling in Structural Integrity.

P.S.: DOI may be included at the end of citation, for completeness.

Book details

Book: Model-based and Signal-Based Inverse Methods

Edited by: Jorge, Ariosto B., Anflor, Carla T. M., Gomes, Guilherme F., & Carneiro, Sergio H. S.

Volume I of Book Series in:

Discrete Models, Inverse Methods, & Uncertainty Modeling in Structural Integrity

Published by: UnB City: Brasilia, DF, Brazil Year: 2022

DOI: https://doi.org/10.4322/978-65-86503-71-5

Fundamental Concepts for Guided Lamb Wave-based Structural Health Monitoring

Roberto Mendes Finzi Neto*[1], Stanley Washington Ferreira de Rezende[2], Jose dos Reis Vieira de Moura Junior[3]

[1]Post-Graduate Program – Mechanical Engineering, Fed. University of Uberlandia, Brazil. E-mail: finzi@ufu.br

[2]Post-Graduate Program – Mechanical Engineering, Fed. University of Uberlandia, Brazil. E-mail: stanley_washington@ufu.br

[3]Post-Graduate Program – Modeling and Optimization, Fed. University of Catalao, Brazil. E-mail: zereis@ufcat.edu.br

*Corresponding author

Abstract

This chapter presents the basic concepts for implementing the guided Lamb Wave method for damage monitoring in mechanical structures. This is one of the structural health monitoring techniques that have been employed in recent years using a network of transducers in order to inspect thin structures. Basically, the methodology allows damage monitoring by comparing the reference signals with the test signals. However, the acquisition systems commonly used in this technique have a high added cost and also require a better level of technical knowledge on the part of the analyst. Thus, this contribution aims to present the development of a low-cost and easy instrumentation system for monitoring structural integrity using Lamb Waves, enabling the use of the technique in field studies, as well as in the context of incipient research in schools.

1. Introduction

Several types of mechanical systems in use in engineering are subjected to critical work regimes in which, combined with possible design errors, can lead to failures, cracks, or damage (Moura Jr, 2008). In this way, the ability to monitor the useful lifetime in which these systems can maintain their operability has been emphasized in the field of structural engineering in recent years. These aspects concern economic, environmental, health, and safety factors.

Thus, in this chapter, we seek to carry out the evaluation of problems related to the scope of structural integrity monitoring, usually defined in the literature as Structural Health Monitoring (SHM). Such methods have the ability to detect and interpret changes in mechanical properties of the structures under study, in order to facilitate the management of the structural life cycle. These generally include steps of data acquisition, filtering, validation, and analysis (Kudela et al., 2018).

The basic principle used by the SHM methodology is that the presence of damage influences the physical and/or geometric properties of the structures, such as stiffness, mass, energy dissipation patterns, boundary conditions and system connectivity. All these elements can negatively affect the final performance of the structure, causing a change in the dynamic response of the system. To do so, it is necessary to compare the two fundamental states of the analyzed structure, that is, the healthy state condition and the damaged state condition (Saravanan; Gopalakrishnan; Rao, 2015).

In carrying out the process of monitoring the states of a mechanical structure, SHM techniques make use of so-called intelligent or adaptive materials, mechanically coupled to these structures (Cui; Liu; Soh, 2014).

Piezoelectric materials are among the main types of intelligent semi structures present in the literature, which are currently used with great efficiency both as sensors and actuators. These, added to a power source and subsequent fault assessment algorithms, allow the continuous monitoring of a given mechanical system over time (Santos, 2004).

In the same way as other non-destructive testing (NDT) techniques, the sensing employed by SHM methods preserve the primary characteristics of the structure after its completion (Soleimanpour; NG, 2017). Sensing can be performed passively, evaluating a certain state of a structure using passive sensors, which are continuously monitored in time and subsequently fed back into the structural system, or active, which employs actuators in order to interact with the interface of the mechanical system.

Piezoelectric wafers (PZT - Plumbum Zirconate Titanate) currently represent the main materials used in the active monitoring of SHM (Venugopal; Wang, 2015).

According to Franco (2009), the main challenge of monitoring structural integrity is the fact that changes in the dynamic response of the systems actually come from the presence of damage, as well as how to identify them. In this context, one of the main SHM methodologies in the time domain that has recently been shown to be efficient in predictive studies is the method based on the so-called Lamb Waves (Pohl et al., 2012).

Although its theoretical basis was founded in the 1920s by Horace Lamb, the Lamb Wave monitoring method has re-emerged in the last three decades as one of the most reliable methods for damage identification (Dalton, 2000). This event is due to the recent technological development of instrumentation systems as well as the need to develop low-cost integrity analysis techniques.

It should also be noted among the characteristics of the SHM technique by Lamb Waves, which is non-destructive, simple instrumentation, and has a broad perspective of applicability with intelligent control systems. These reasons attract their use in regions of difficult access and high implementation cost, such as in naval, automotive, space, and/or aeronautical structures (Leucas, 2009).

However, the physical experimentation of this monitoring technique is often reduced due to the process of building the scientific base. Such a situation often makes its understanding and application deficient. Therefore, the main objective of this chapter is to apply concepts already widespread in the scope of integrity analysis and a few practical details in SHM in an attempt to build a low-cost experimentation model of the structural integrity monitoring technique by Lamb Waves. (Moura Jr, 2008; Ledesma, 2015).

2. Smart Materials and Lamb Waves Technique

Piezoelectric transducers from their conception stage to modern times have been widely used in different types of electronic devices. This fact is due to that these semi structures have a low manufacturing cost and reduced dimensioning, combined with low operational energy consumption that makes them attractive in engineering applications (Kobayashi et al., 2009).

According to Afshari (2012), the piezoelectricity effect was developed at the end of the 19th century by Jacques and Pierre Curie. In their work, they identified that certain types of materials, when subjected to electric fields at high temperatures, showed a relative deformation of their dimensions. This property was later called Curie Temperature and is the temperature at which the material spontaneously loses its initial polarization and, consequently, its piezoelectric property. Thus, it has been called piezoelectric material any material that has the ability to relate different electrical potentials in mechanical efforts applied to it, or inversely, measure deformations generated in the material from subjected electrical potentials (Lu et al., 2017). The direct effect is the process of formation of a potential difference between the dipoles of a piezoelectric transducer when they are subjected to mechanical deformation. On the other hand, the inverse effect consists of the mechanical deformation of the transducer by imposing a potential difference (Lu et al., 2017). This relationship obtained between the applied electric field and the subsequent mechanical deformation of a given structure can be quantified according to equation (1).

$$\epsilon_{ij} = \rho_{ij}\left(\frac{v_i}{l}\right) \tag{1}$$

where ϵij is the piezoelectric modulus, *i* is the direction of the applied electric field, and *j* is the direction resulting from the normal strain; *v* is the voltage applied to the PZT patch in the electric field direction *i* and *l* is the patch thickness.

Through an initial formulation proposed by Devonshire, he determined that the characteristic relationships of dielectric materials precede the total energy of the system. This means that it is possible to understand the phenomenological relationships of the direct and inverse piezoelectric effects of a given electromechanical system (Fu; Cohen, 2000). Still, even considering the responses of these structural applications very close to linearity, when performing procedures with high levels of excitation, at high frequencies, the piezoelectric elements still showed non-linearity characteristics, making the modeling complex. Thus, applications involving piezoelectricity effects are generally restricted to the linear laws formulated by Voigt, where the direct and inverse effects follow, respectively, equations (2) and (3) (Franco, 2009).

$$D_m = \epsilon^T_{mn} E_n + d_{mkl}\sigma_{kl} \tag{2}$$

$$e_{ij} = s_{ijkl}\sigma_{kl} + d^T_{mij} E_m \tag{3}$$

where, *D* and *E*(n/m) represent, respectively, the displacement vector and the electric field vector of the PZT patch; ϵ^T_{mn} and *d* represent the material's dielectric tensor and the piezoelectric voltage tensor; the ceramic material strain and the sigma stress are related by the applied longitudinal tensor s.

At this moment, it is possible to understand that characteristics of the direct effect of piezoelectric materials allow their use as sensors, as the property resulting from the inverse effect allows the description of the device as an actuator (Islam; Huang, 2016). However, to perform an efficient fault identification, the electromechanical coupling of such structures must be designed in a way that does not significantly influence the dynamic response of the structural system.

Among the main types of piezoelectric materials presented in the literature that have subsequently been used efficiently in fault diagnosis are:

- lead titanate-zirconate (PZT) patches: ceramic material that generally has greater stiffness than the holding structure, allowing an effective electromechanical coupling to identify damage.
- Polyvinylidene Fluoride (PVDF) polymers: greater ductility compared to PZT patches and also greater elasticity than common engineering structures, making their use as actuators inefficient.

In the literature, there are two possible approaches that correlate the Lamb Waves technique to the use of piezoelectric materials for the fault identification process, especially in relation to the use of PZT patches. Such approaches are called pulse-echo and pitch-catch (Mei; Giurgiutiu, 2018), and both are respectively represented in Figure 1.

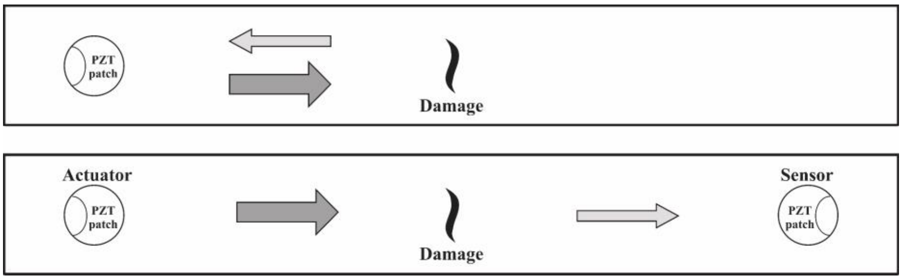

Figure 1: Pulse-echo and pitch-catch approaches in Lamb Waves techniques.

The pulse-echo approach employs only a single patch in order to interact with the host structure and receive its dynamic response. The pitch-catch, on the other hand, employs two or more piezoelectric transducers, interacting alternately (one as sensor and the other as actuator) in the gathering process (Zhang et al., 2016).

However, some noise can be acquired during the data collection procedure due to intrinsic (electronic components) and environmental (temperature) aspects that involve the experimental procedure. These noises can interfere to indicate false positives in the damage inference process. Thus, it is necessary to apply extraction methods to obtain information from the wave propagation medium in the structures under study. In this context, Wavelet Transforms have been shown to be very useful for the analysis of non-stationary signals, making their use widespread in the most diverse areas, including the analysis of structural integrity.

3. Continuous Wavelet Transform (CWT)

Wavelets are representations of wave functions of short duration with sudden changes in amplitude, proportional to their fast decay in time. This feature of signal energy limitation gives Wavelets a compact aspect in their use, being useful to signal processing, especially to non-stationary signals (Park et al., 2007).

The wavelet transform mathematical approach is based on scalar representation and maps the signal into the resolution-scale domain, alternatively to the frequency domain of classical Fourier analysis. Thus, all scales in the resolution-scale domain, without exception, have their frequency equivalence in the time-frequency domain (Debnath; Shah, 2002).

One of the main tools that make up the Wavelet theory, the Continuous Wavelet Transform (CWT) describes the union of a set of base functions resulting from different displacement and dilation operations of the main Wavelet in the scale resolution domain. This main Wavelet is called Mother Wavelet $\Psi_{(a,b)}$ and is described by equation (4).

$$\Psi_{(a,b)}(t) = \frac{1}{\sqrt{a}}\Psi\left(\frac{t-b}{a}\right) \tag{4}$$

where *a* is the scale parameter that are compressed or extended versions of the Mother Wavelet function and *b* is the displacement parameter, positioning the function in the temporal domain (Domingues et al., 2016). These compressed and extended versions of the Mother Wavelet function can be obtained by convoluting functions belonging to Wavelets families in time.

Therefore, the decomposition of a signal *f(t)* resulting from the application of CWT at different frequencies allows us to obtain a family of scales in the Wavelet Domain. This decomposition is carried out according to equation (5).

$$CWT_{(a,b)}(t) = \frac{1}{\sqrt{a}}\int_{-\infty}^{\infty} f(t)\Psi\left(\frac{t-b}{a}\right)dt \tag{5}$$

As the displacement parameter changes, the signal is analyzed locally around it. This means that the Wavelet function molds itself to different parts of the signal in order to allow detection of the characteristic frequencies of each region.

Figure 2 illustrates the relationship between the multiple scales of the Wavelet domain and their subsequent equivalence in the power spectrum. Furthermore, in this image, the process of abstraction of a time-varying signal by the CWT technique is also conceptually presented.

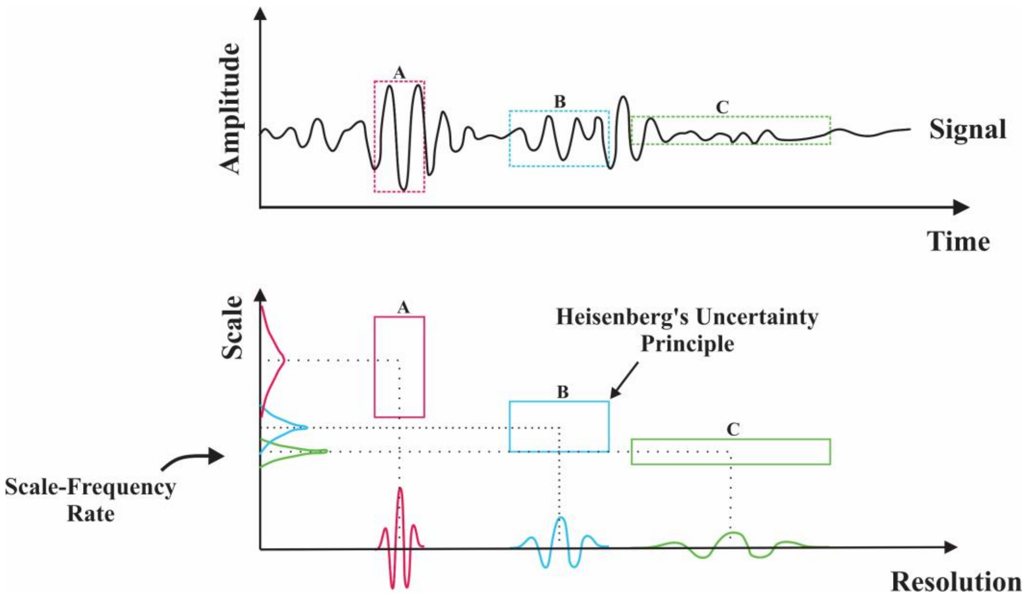

Figure 2: the process of abstraction of a time-varying signal by the CWT technique.

In general, the most used continuous wavelets in the signal analysis are the functions of the Complex Morlet family. These functions provide information about the phase, modulus, and discontinuous periods of the signal. Morlet Wavelets can be obtained by multiplying a complex exponential with a modeling Gaussian window, according to equation (6).

$$\Psi(t) = \int_{-\infty}^{\infty} \left(e^{-iwt}\right)\left(e^{\frac{t^2}{2\sigma^2}}\right) dt \tag{6}$$

where σ is the Gaussian standard deviation correlated to the Heisenberg uncertainty principle present in the Wavelet function. This parameter provides information on the quality of the time-frequency relationship of the signal analysis windows. High values for σ allow obtaining better resolutions in the frequency domain, while small values lead to better temporal resolutions of the signal (Debnath; Shah, 2002). Figure 3 illustrates Morlet's Wavelet function ranging from 0 to 1000 seconds. It can be seen in Figure 3 that the Morlet function presents a sudden scalar variation in a short period of time (around -2 and 2) and null at other moments.

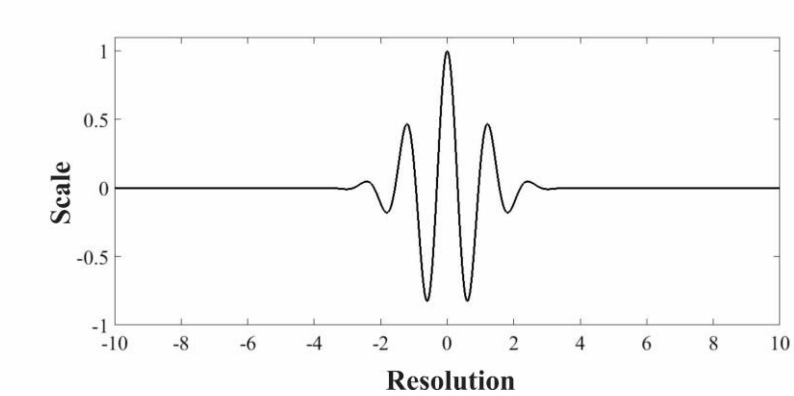

Figure 3: Morlet's Wavelet function.

The Wavelet approach differs from the Fourier methodology because it is locally restricted to a single region, while Fourier uses infinite oscillatory functions obtained from families of sine and cosine. Thus, the approach using CWT suggests being able to extract different frequency bands, as well as their respective energy contributions in the formation of the vibration signal of a given structure (Domingues et al., 2016). Thus, the application of CWT with integrity monitoring techniques based on Lamb Waves allows monitoring failure behaviors.

4. Fundamentals of Lamb Waves

Recently seen as one of the most widely used methods in identifying damage in structural dynamics, Lamb waves use a system composed of transducers, usually piezoelectric. This system sends mechanical voltage waves in the host structure and, based on the comparison of variations between the received signals, it monitors the presence of damage (Rocha, 2017).

Based on the movement of the structure, the Lamb Wave method can be understood as the superposition of two basic modes of vibration. These are the longitudinal wave propagation mode and the transverse wave propagation mode.

In longitudinal propagation, the movement applied to the material particles is defined as parallel to the direction of the force that runs through the structure. In transverse propagation, this movement is perpendicular to its direction. Thus, the coupling of such basic vibration modes enables the method the possibility of inspecting a large coverage area, making it attractive to several engineering applications (Sun; Zhang; Rose, 2005).

There are several mathematical equations capable of obtaining the modes: longitudinal and transverse wave propagation, each with its own particularity (Possani et al., 2017; Santos, 2004). However, among the main methods used efficiently in the literature, there is one based on scalar and vector potential fields of the wave. These are expressed according to equations (7) and (8), respectively:

$$\frac{\partial^2 \varphi}{\partial x^2} + \frac{\partial^2 \varphi}{\partial z^2} = \frac{\partial^2 \varphi}{v_L^2 \partial t^2} \tag{7}$$

$$\frac{\partial^2 \psi}{\partial x^2} + \frac{\partial^2 \psi}{\partial z^2} = \frac{\partial^2 \psi}{v_T^2 \partial t^2} \tag{8}$$

where φ and Ψ represent the potential displacement functions; v_L and v_T are, respectively, the longitudinal and transverse propagation velocities of the wave in the material; x is the coordinates of the wave propagation direction, z is the coordinates of the normal direction on the surface of the structure, and t is the propagation time. The longitudinal and transverse propagation velocities can be obtained, respectively, according to equations (9) and (10) (Santos, 2004).

$$v_L = \sqrt{\frac{E(1-\sigma)}{\rho(1+\sigma)(1-2\sigma)}} = \sqrt{\frac{2\mu(1-\sigma)}{\rho(1-2\sigma)}} \tag{9}$$

$$v_T = \sqrt{\frac{E}{2\rho(1+\sigma)}} = \sqrt{\frac{\mu}{\rho}} \tag{10}$$

where E is the modulus of elasticity, μ is the shear modulus, σ is the Poisson's coefficient and ρ is the density of the material that constitutes the structure.

Using the Euler formula and subsequent simplification processes, the sinusoidal solutions found for the potentials expressed in equations (7) and (8) are given by equations (11) and (12).

$$\varphi = \left(A_1 sin\left(pz\right) + A_2 cos\left(pz\right)\right) e^{-i(kx-\omega t)} \tag{11}$$

$$\psi = \left(B_1 sin\left(qz\right) + B_2 cos\left(qz\right)\right) e^{-i(kx-\omega t)} \tag{12}$$

where A_1, A_2, B_1, and B_2 are constants defined according to the boundary conditions of the system under study, k represents the number of pulses that, as well as the parameters p and q, are obtained by equations (13), (14) and (15), respectively.

$$k = \frac{2\pi}{\lambda} \tag{13}$$

$$p = \sqrt{\frac{\omega^2}{v_L} - k^2} \tag{14}$$

$$q = \sqrt{\frac{\omega^2}{v_T} - k^2} \tag{15}$$

where λ represents the wavelength and ω the angular frequency obtained by $2\pi f$, where f is the cutoff frequency.

In this scenario, the literature describes two patterns for the combination of these propagation modes in an isotropic material, simultaneously, correlating them to the structural characteristic movement, called symmetric and anti-symmetric patterns.

Considering an isotropic plate as propagation material, the system boundary conditions can be easily obtained using the Rayleigh-Lamb equations (Corrêa, 2014). The Rayleigh-Lamb equations for symmetric and antisymmetric modules are expressed as equations (16) and (17), respectively.

$$\frac{tan\left(qh\right)}{tan\left(ph\right)} = \frac{-\left(k^2-q^2\right)^2}{4qpk^2} \tag{16}$$

$$\frac{tan\left(qh\right)}{tan\left(ph\right)} = \frac{-4qpk^2}{\left(k^2-q^2\right)^2} \tag{17}$$

In symmetrical modules, the elements that move in the material have a certain conformity in relation to the median plane of the structure, and these are commonly used for failure analysis in metallic structures. In antisymmetric modules, the elements interact alternately in relation to the median plane of the structure, being used in composite structures (Shen, 2014). Both patterns can be graphically visualized in Figure 4.

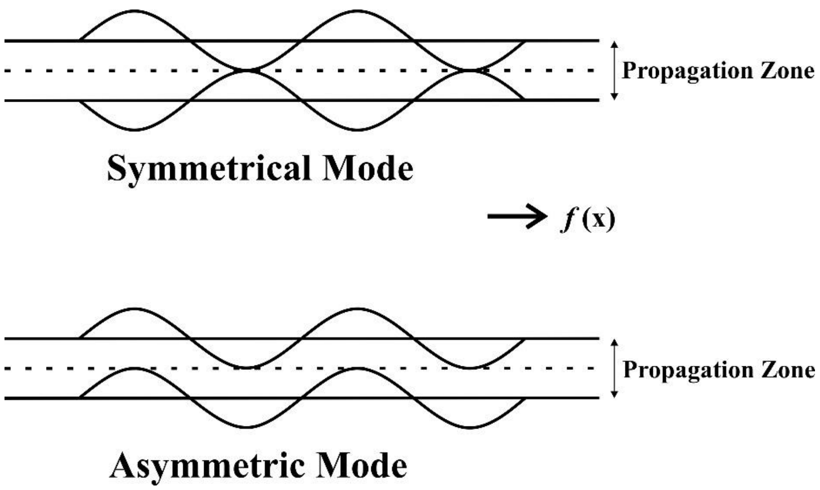

Figure 4: Symmetric and anti-symmetric patterns.

There are infinite wave propagation modes, symmetric and anti-symmetric, able to traverse structural materials. They can be obtained by different cutoff frequencies while becoming dependent on the specific properties of the materials that compose them (Qiao; Fana, 2014). The propagation modes are commonly represented in the literature by S_i (symmetric) and A_j (anti-symmetric), where i and j are the orders of each module.

Cardoso et al. (2012) used the A_1 and S_0 propagation modes in order to inspect possible corrosion in carbon steel tubes and aluminum plates. Therefore, the displacement curves of the propagation modes in these two structures and the groups of longitudinal propagation modules in the tubes were qualitatively evaluated. In addition, a quantitative analysis of phase velocities was performed, using a difference factor. Oliveira (2015) compared the same symmetric S_0 mode of Lamb Waves to the quasi-Scholte mode in studies of metallic plates submerged in a viscous fluid. Both described that the Lamb Wave integrity monitoring method is more effective than the frequency domain-based methods in terms of location, severity, and type of damage.

However, it is important to note that the abstraction of information from the waves obtained in the execution of experimental processes becomes the main hesitation in applying the method. This is due to its assessment, which is a complex task, as Lamb's guided waves are relatively influencing of the wavelength and cut-off frequency (Mechbal; Rebillat, 2017). In this sense, in order to abstract characteristics regarding the propagation medium, signal processing algorithms can be used, such as the Fast Fourier Transform (FFT) and the CWT. The use of this type of algorithm enhances the capabilities of the Lamb Waves fault identification method, enabling the extraction of characteristic frequencies in the case of

FFT, or even finding signal energy scales in the time domain for CWT (Franco, 2009). Also, it should be noted that the current data acquisition systems used in monitoring by Lamb Waves have a high operational cost added to a robustness that complicates its use in field analysis, as well as its large-scale evaluation.

5. Damage Index for Lamb Waves

In this section, we will briefly discuss the measurement of structural integrity using lamb waves. Initially, it is considered that the mechanical system is properly instrumented with piezoelectric transducers (actuator-sensor) with adequate electromechanical coupling. The experimental procedure of integrity inspection by Lamb Waves starts with the determination of the waveform to be used for system excitation (Leão et al., 2012).

Therefore, to configure the waveform to be used in the mechanical excitation process, three main factors of the wave must be taken into account, namely: amplitude, frequency, and propagation period. The first factor is defined considering that the insertion of energy into the system allows the propagation of the signal throughout the evaluated structure, without its complete attenuation (Leucas, 2009).

It should be noted that the material used in PZT patches has a relative linearity limit, thus making the signal amplitude typically lower than *5Vpp*. For the other wave parameters, although there are optimization methods to define them, in practice these are obtained by trial-and-error processes.

Having performed the mechanical excitation of the evaluated structure, the response signals are then measured by the sensor transducer and subsequently processed by data extraction or processing tools, such as CWT. This treatment leads to obtaining a signal energy scalogram, in which the scale with the greatest contribution is directly associated with the structural characteristic movement.

From the wavelet scale with the greatest contribution to the composition of the signal, it is possible to abstract several characteristics such as signal energy, phase and group velocities, propagation period, and peaks of maximum and minimum of the wave. Therefore, using such tools, it is possible to relate the different states of the structure from the variation of these wave aspects (Palmos, 2009).

However, to perform a quantitative analysis of these aspects of the signal, failure indexes called damage metrics are commonly used. The most common metric for the Lamb Waves method is the Damage Index (DI) as presented by equation (18) (Cheraghi; Taheri, 2007).

$$DI = \left| 1 - \frac{\int_{t_0}^{t_n} CWT_D(t, a_0)\, dt}{\int_{t_0}^{t_n} CWT_B(t, a_0)\, dt} \right| \qquad (18)$$

where a is the scale with the greatest contribution to signal composition, D index represents the signal to be evaluated and B index represents the baseline signal.

According to the equation, it can be seen that the DI metric performs a comparison of the propagated energy variation between the different states of the structure. In this way, the metric values will vary between *0* and *1*, with values close to *1* meaning the presence of damage.

6. Lamb Waves Experimental Setup

In recent decades, there has been a growing search for new instrumental approaches (portable and with lower added cost) for monitoring structural integrity. However, alternative systems that are currently described in the literature still require a great deal of technical knowledge on the part of analysts and researchers, as well as on the areas related to the maintenance and set of electronic systems (Moura Jr, 2008; Wang et al., 2018). In the following section, some works developed in the last decade will be presented to illustrate some possible experimental approaches.

This section will clarify the process of structural health monitoring using the Lamb Wave method, covering all the necessary tools for its application. Since there are different possible equipment setups for the application of the technique, this section will present an elementary and low-cost approach, easy to implement by the user, without the need for great technological knowledge.

Initially, it is necessary a source of energy generation to promote the excitation of the structure, an analyzer to measure the sensor signal, and a computational interface to store it. This approach will also require PZT patches such as sensors and actuators. Aiming at the aspects of low cost and ease of implementation mentioned above, the following items were used in this work:

- UDB11008S wave generator;
- 2530 B&K Precision digital oscilloscope;
- 2 PZT patches (20 mm in diameter by 3 mm thick);
- computer (Software: EasyScope) for data collection, storage, and processing.

The UDB110x (S) series consists of frequency generators up to *8MHz* with an integrated circuit in the FPGA category. They are direct digital synthesis (DDS) alternating voltage generators with standard sine, square, triangle, and sawtooth waveforms. These generators are characterized by having high stability and low distortion, in addition to being able to regulate the amplitude and DC polarization of the output signal.

The UDB11008S generator has a sweep function, allowing you to freely define the interval and the sweep time (sweep). The output signal amplitude can reach a maximum of *9Vpp* and a minimum of *10mVpp*. However, because the PZT patches used in this example have high stiffness and small thickness, this function was set to a minimum output (*10mVpp*) (Tsuruta et al., 2008).

In the measurement step, the B&K Precision 2530 oscilloscope combines characteristics such as high performance and low cost. Since this part of the system in the literature shows itself as the one with the highest aggregate cost, this should be the item with the most careful choice. This equipment is capable of reading signals with a relative bandwidth of up to *25MHz*, with a sampling of *500 MSa/s*.

In the acquisition step, the integration between the oscilloscope and the EasyScope software allows you to explore functionalities such as collection, filtering, and storage (up to *32* automatic measurements) of signals with sizes of *500* (high-pass) or *32000* (low-pass) points. It is still possible to perform an FFT on the sample signal with different decomposition windows in order to perform both time and frequency domain analysis.

In this next step, the generator and the analyzer are connected to the two PZT inserts coupled to the structure. In the case under study, the pitch-catch configuration is used, as presented in section 2 (YU et al., 2012). With the connection of the acquisition system to the computer through a USB port, full manipulation of the system via software is possible.

An important feature of the UDB11008S generator is that it operates with a *5V* supply, allowing its use in-field analysis. Figure 5 presents the scheme of the acquisition system developed in this work, where the monitored structure is illustrated by a plate.

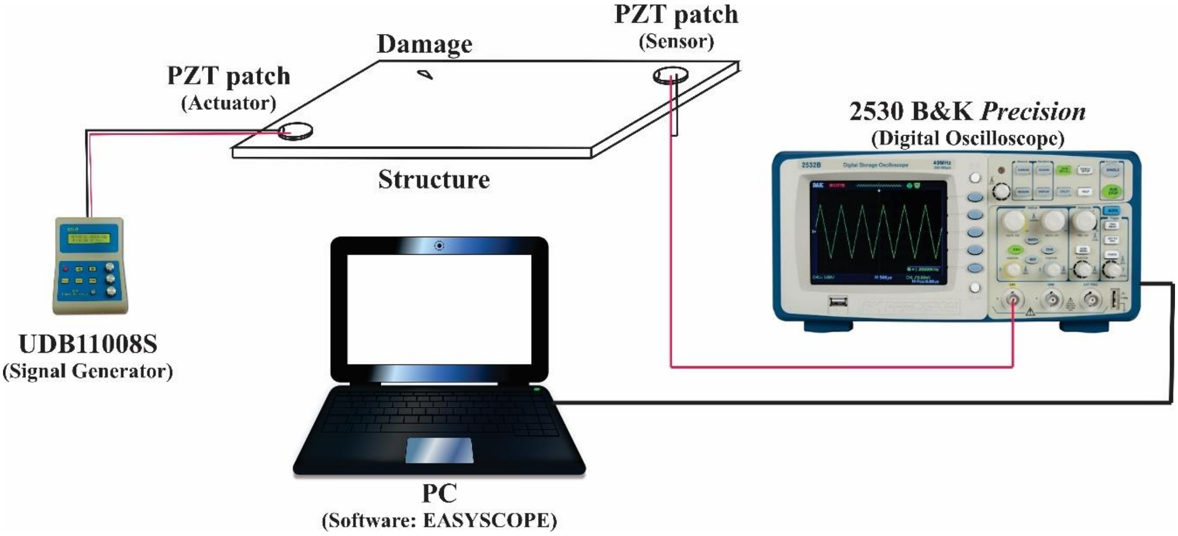

Figure 5: Low-cost Lamb Waves Experimental Setup.

The first instrumentation step of the acquisition system developed in this work consists of the electromechanical coupling between the piezoelectric chips and the structure to be monitored. For this, both PZT ingots must be bonded to the structure with a thin layer of epoxy adhesive, taking approximately 24 hours for effective curing. A simplified description of the piezoelectric patch bonding process can be seen in Figure 6.

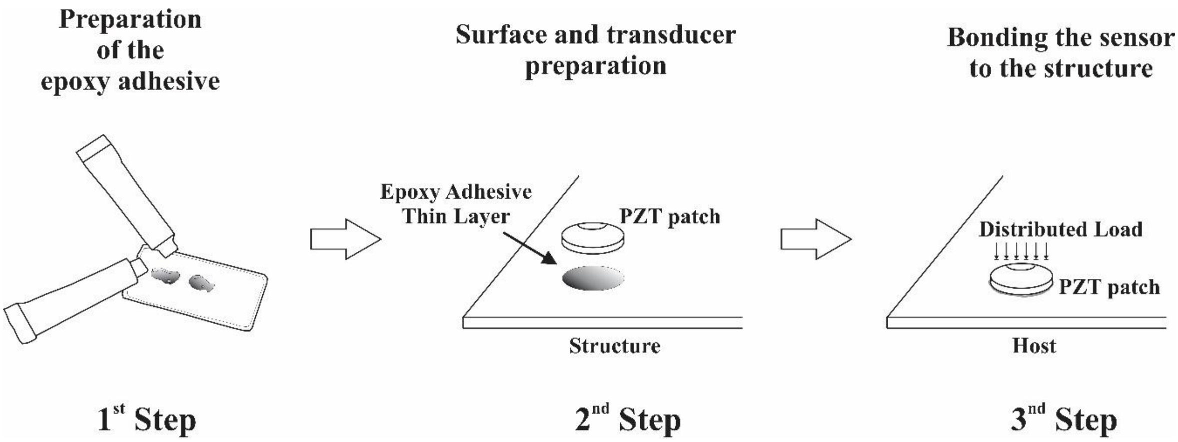

Figure 6: Piezoelectric patch bonding process.

The epoxy adhesive was used due to its mechanical properties such as 1) high stiffness compared to other types of glue, allowing an efficient electromechanical coupling; 2) resistance to high temperatures, remaining unchanged up to 70º C (Overly; Park; Farrar, 2007). Furthermore, the adhesion of the transducers to the structure must be performed in a way that does not significantly interfere with the dynamic response of the system, thus ensuring that the presence of damage is the only factor for the variation of Lamb Waves.

The definition of the best coupling positions of the transducers in the structure takes into account its geometry, dimensions, contour shapes, the excitation capacity of each PZT patch, and the prerogatives of the pitch-catch configuration, that is, linear positioning between the actuator and sensor.

After the step of bonding the patches, two wires must be soldered to the electrodes of each piezoelectric component. Then, the PZT patch actuator wires are connected to the probes of the UDB11008S wave generator, which are connected to its output terminal (OUT). Now, the PZT patch sensor wires are connected to one of the channels (CH1 or CH2) of the digital oscilloscope, and this is also done with the aid of probes. Figure 7 presents the schematic representation of the connections of the transducers to the electronic components.

After the acquisition system is properly connected, the process of calibration and configuration of its electronic components begins, that is, the configuration of the wave generator and digital oscilloscope.

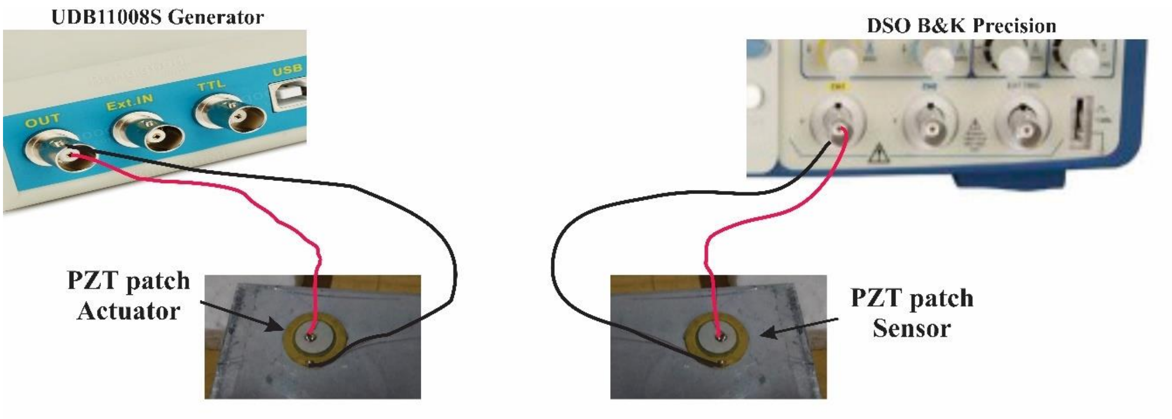

Figure 7: Graphic representation of the process of connections between PZT inserts and acquisition system equipment.

Wave generators currently play an important role in the study of electronic measurement circuits. They make it possible to analyze and manipulate the parameters of interest from previously generated reference signals. Also, with the development of digital technology, analog-to-digital converters began to create high-precision signals, mainly through the use of DDS technology. In this context, the frequency generators belonging to the UDB110x (S) series have shown great applicability in engineering and computing studies (Chen; Chen, 2011).

The UDB11008S signal generator, belonging to the commented series, allows creating alternating voltage waves in standard sine, square, triangular and sawtooth waveforms with high stability and low distortion. Figure 8 presents the schematization of the features of this generator, and each feature is described later.

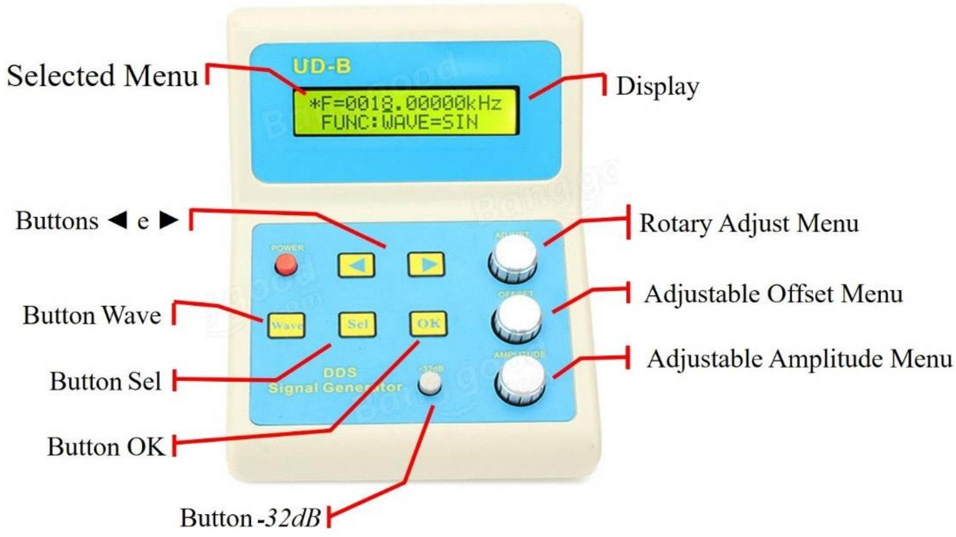

Figure 8: Function Generator - UDB11008S model.

The *Sel* key carries out the selection procedure between the function menu and the output frequency, in which the chosen functionality is represented by the * operator on the display. When the selected operation is the output frequency setting, the left and right arrows allow scrolling between the chosen frequency numbers. Here, the *Adjust* menu allows the increase or decrease of this value.

Pressing the *OK* button switches between the frequency measurement scales that the signal generator is able to generate (Hz, kHz, and MHz). It is worth mentioning that the UDB11008S generator is capable of generating waves with a frequency of up to 8MHz.

When the functions menu is chosen, the left and right arrows allow switching between functions previously stored in the generator's memory. Then they modify the control characteristics of the output wave and the external measurement. The functions available in the generator's memory are:

- *WAVE* – allows modifying the generated wave pattern by selecting and pressing the *OK* button. The UDB110x (S) series is capable of generating standard sine (*SIN*), square (*SQR*) and triangular (*TRI*) waveforms;
- *DUTY* – adjusts the duty cycle of square and triangle waveforms. When the triangle waveform is chosen, imposition values greater than 50% cause the waveform to change to a rising sawtooth, while values less than 50% cause the waveform to change to a descending sawtooth;
- *COUNTER* – represents a counter that starts from an external pulse being measured by the *Ext.IN* input terminal. The value starts to be shown on the display, while the *OK* button allows resetting the counter;

- *EXT.FREQ* – allows measurement of external frequencies from the *Ext.IN* input terminal;
- *SAVE* – allows the storage of base parameters. The stored data is the current frequency value, waveform, and duty cycle. The UDB11008S model has 10 memory storage positions, which can be changed and loaded at any time. For data storage, the following steps must be followed:
  1. Choose the current frequency and data (WAVE and DUTY);
  2. Choose the memory location to store the data;
  3. Press *OK* button to save.

  It is worth mentioning that the memory position *M0* is the wave generator's default, being called at all times during its initialization. Furthermore, the memory variables *M1* and *M2* (frequencies stored in the same way as described) are the frequency values used in the sweep (without using the *WAVE* and *DUTY* data).

- *LOAD* – loads the data stored in a given memory by the *SAVE* function;
- *TIME* – sets the sweep time to be used in the sweep;
- *SWEEP* – performs a sweep, adding the frequency value gradually over time. The start frequency value is delimited by the variable *M1* while the stop frequency value is delimited by the variable *M2*. These are obtained according to the *SAVE* submenu. The increment frequency value is defined according to the scan time previously defined in the *TIME* function of the submenu. To generate a single pulse, the values of variables *M1* and *M2* must be the same, and if these variables are not defined in memory, the standard sweep will be performed starting from *0kHz* to *10kHz* with a step of *0.1Hz*;

The *Wave* key on the function generator allows direct switching between the different waveforms (sine, square, and triangle). Meanwhile, the *OFFSET* and *AMPLITUDE* adjustment menus allow, respectively, to adjust the DC polarization and amplitude of the output signal. The *-32 dB* button attenuates the output signals to values below 10mVpp.

Based on the physical instrumentation process of the developed system, the generator calibration will depend on the wave properties to be studied. This by itself can be (also known as time-of-flight - TOF), or by means of a frequency sweep, in order to check the variation of resonant frequencies.

Figure 9 presents a flowchart for carrying out the wave generator configuration in each particular case. However, in both cases, frequencies higher than 10kHz and lower than 40kHz are chosen, since in this frequency range it is possible to assess incipient damage (MOURA JÚNIOR, 2008).

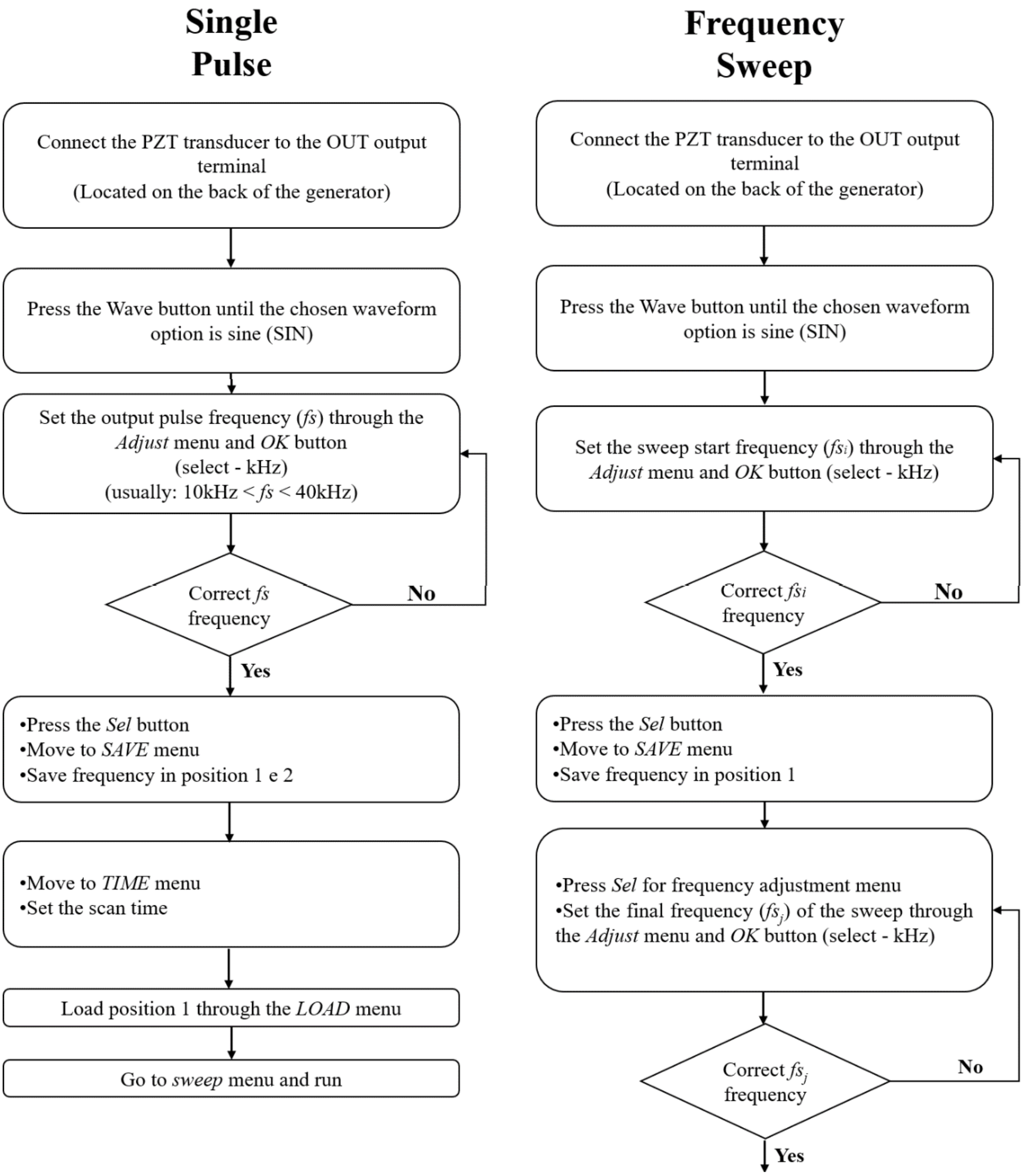

Figure 9: flowchart for setting up the UDB11008S wave generator.

During the studies of Lamb Waves, the standard sine wave format is generally used, since it makes it possible to obtain the phase and period of the wave more easily compared to other patterns.

After a reference signal is sent by the function generator and subsequently propagated through the structure under study, it will be captured by the PZT patch sensor coupled directly to the channels of the digital oscilloscope. This oscilloscope will graphically display the measured signal and then store it. Therefore, it is necessary to configure and define the parameters of this other device.

The Digital Storage Oscilloscope (DSO) is a flexible instrument that aims to measure measurements and data regarding wave aspects. This makes it possible to graphically analyze the electrical signals in the time domain and later store them in external memory (USB) (Cardoso; Silva; Segundo, 2017).

In most applications, the DSO acquires signal samples and represents them virtually on the display, where the vertical axis expresses the measured signal amplitude (Volts/Div) and the horizontal axis the wave scan time (Sec/Div). Figure 10 presents a schematic of the digital oscilloscope parts while the functions are given in Table 1.

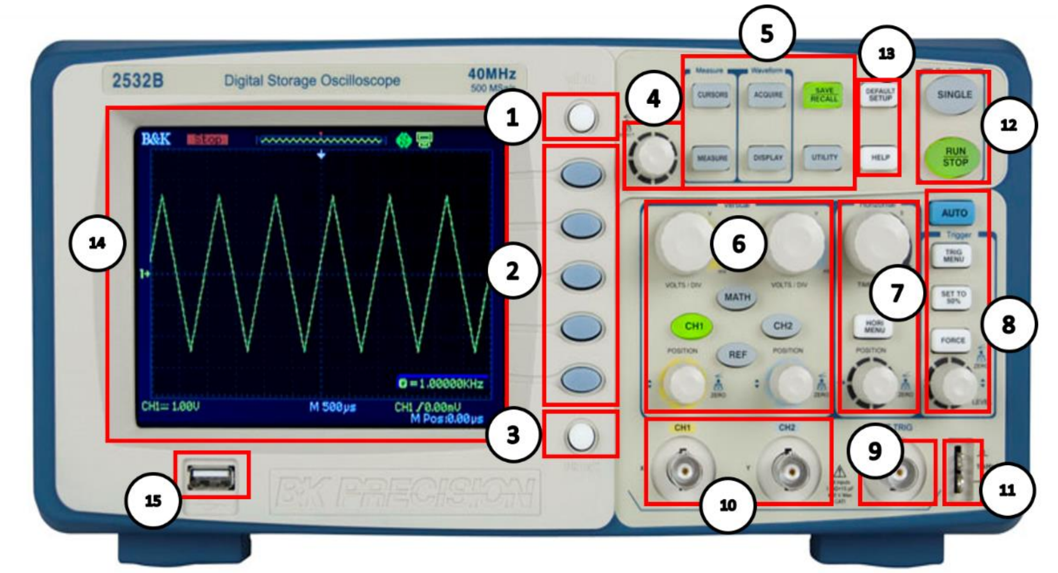

Figure 10: B&K Precision Oscilloscope – measurement of the sensor.

Table 1: B&K Precision Oscilloscope functions

Item	Function Name
1	On/Off Menu
2	Selection Buttons
3	Print
4	Universal Menu
5	Measurement and Acquisition Functions
6	Vertical Controls (CH1 and CH2)
7	Horizontal Control
8	Trigger Menu
9	Channel for External Calibration
10	Input Channels (CH1 and CH2)
11	Compensation terminal
12	Acquisition Control
13	Default and Help Buttons
14	LCD Display
15	USB input

The first step to be adopted, before any measurement test, is the calibration of the system to be used. This procedure can be performed by pressing the *Default Setup* button, located at 13, and later, by adjusting the signal obtained by the probe, which must be connected to the *Compensation Terminal*.

Vertical Controls modify both the magnification of the waveforms, which are obtained by the *Input Channels* and their positioning on the vertical axis. Also, the *CH1* and *CH2* buttons allow the visualization and application of digital filters on the sampled signals. The relationship between different filter types and menu options is shown in Table 2.

Table 2: B&K Precision Oscilloscope filters

Menu icon	Filter type
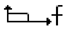	Low-pass
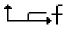	High-pass
	Band-pass
	Notch/Band-reject

The choice of filter type is directly linked to the frequency range to be used in the experiment. Thus, because SHM methods commonly work at high frequencies, this functionality must be set to the high-pass filter type (Leucas, 2009).

In addition, the *MATH* button allows the use of mathematical operations between the multiple channels of the oscilloscope, one of which is the fast Fourier transform. The *REF* submenu displays up to two reference signals for the data to be measured, thus enabling a direct qualitative comparison between the states of the structure, with and without damage.

The *Horizontal Control* provides temporal manipulation of the sampled data on the LCD display. Here, the *Time/Div* and *Position* buttons allow, respectively, the definition of the sampling rate of the signal and its subsequent positioning in the time domain.

The *Menu Trigger* is responsible for synchronizing the acquisition of waveforms when they exceed a given threshold amplitude value. Such functionality allows the sampling of periodic signals, as well as their stabilization in the data acquisition process. Among the forms of synchronization in the *Menu Trigger* are:

- *Trigger Edge* – represents the process of acquiring a given signal when one of its points exceeds the threshold value in a specific direction, be it rising edge or falling edge. The deflection edge Trigger mode is the most used in Lamb Wave SHM studies.
- *Trigger Pulse Width* – delimits the measurement process based on the data collection trigger time with the width of the sampled wave pulse.
- *Trigger Video* – uses NTSC (525 lines of resolution) or PAL (625 lines of resolution) video standards to carry out the data verification process.
- *Trigger Slope* – relates the data acquisition process to the ascent or slope velocity of the measured signal.

When the *SET TO 50%* key is pressed, the digital oscilloscope will perform a quick wave stabilization process based on the measured voltage midpoint. However, such functionality only becomes applicable when a signal is emitted in the *Channel for External Calibration*. The *FORCE* button allows the direct acquisition of waveforms, without the need to detect a trigger threshold value.

The set of buttons present in *Measurement and Acquisition Functions* enable analytical manipulation of the signals sampled on the display, as well as data storage on a flash drive.

To carry out the storage process via physical device, the following steps must be performed on the instrument:

Initially, the flash drive, to be used for storage, must be plugged into the *USB Input* of the digital oscilloscope and wait until it is recognized. If recognition does not take place, a quick audible alert will be emitted by the DSO and, later, the message *"USB Flash Drive is not connected!"* will appear in the lower corner of the display.

With the flash drive recognized by the DSO, as a second step, press the *SAVE/RECALL* key in 5. This is responsible for displaying the storage functions menu.

Different storage options can be performed by DSO B&K Precision from this step, having different peculiarities. Table 3 briefly presents the relationship between the storage options and the subsequent steps that must be taken to save the data.

Table 3: B&K Precision Oscilloscope storage options.

Option	Details	Next Steps
Config	This option stores data in the DSO's internal memory. The B&K Precision oscilloscope has up to 20 positions available for data storage.	1. Select the *Device* option; 2. Choose the memory option to be stored; 3. Select the *Save* option.
Waveform	This option stores the signal image in the DSO's internal memory. The B&K Precision oscilloscope has up to 10 positions available for image storage.	1. Select the *Device* option; 2. Choose the memory option to be stored; 3. Select the *Save* option.
Image	This option stores the image of the signal sampled on the display in a flash drive memory.	1. Press *Save. image*.
CSV	This option stores the wave data (amplitude, time and others) on the flash drive with .csv extension	1. Set the data length option to Display; 2. Press the *Save* option; 3. Choose the name and directory on the flash drive; 4. Press *Save*.
Factory	This option restores the factory parameters of the DSO's internal memory, that is, the option performs the cleaning of the internal memory.	1. Press *Restore*.

Assuming that Lamb Waves use feature extraction methods (CWT) and subsequent damage quantification algorithms, the most used storage form in SHM procedures is the CSV option. This enables the physical storage of the points that compose the signals for further analysis in a computational environment.

When pressing the *CURSORS* key on the DSO panel, the *Selection Buttons* allow the transition between the different cursor options available. With these buttons, it is possible to measure both the signal amplitude variation and the wave periods.

The *MEASURE*, *DISPLAY*, and *UTILITY* buttons allow, respectively, the visualization of the current wave data, the format of displaying the equipment interface, and the configuration of the firmware and system utilities (language, audio, and others).

Figure 11 shows the flowchart for performing the B&K Precision digital oscilloscope configuration via physical equipment.

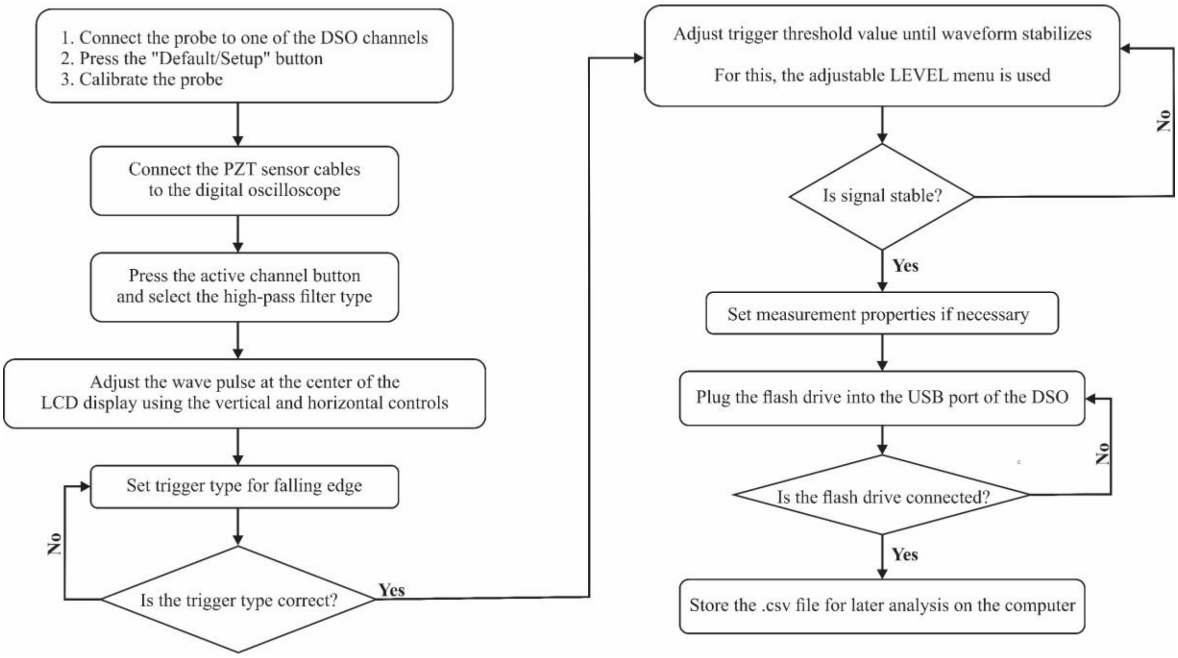

Figure 11: flowchart for B&K Precision Oscilloscope configuration.

7. Experimental Case Study

The experimental procedure adopted in this case study aimed to identify the presence of damage in an aluminum plate with 2 mm thickness and geometry as shown in Figure 12. To monitor this structure, three buzzer-type PZT patches were used, with a geometry of 20 mm in diameter and 0.35 mm in thickness, considering the pitch-catch coupling configuration (Figure 1).

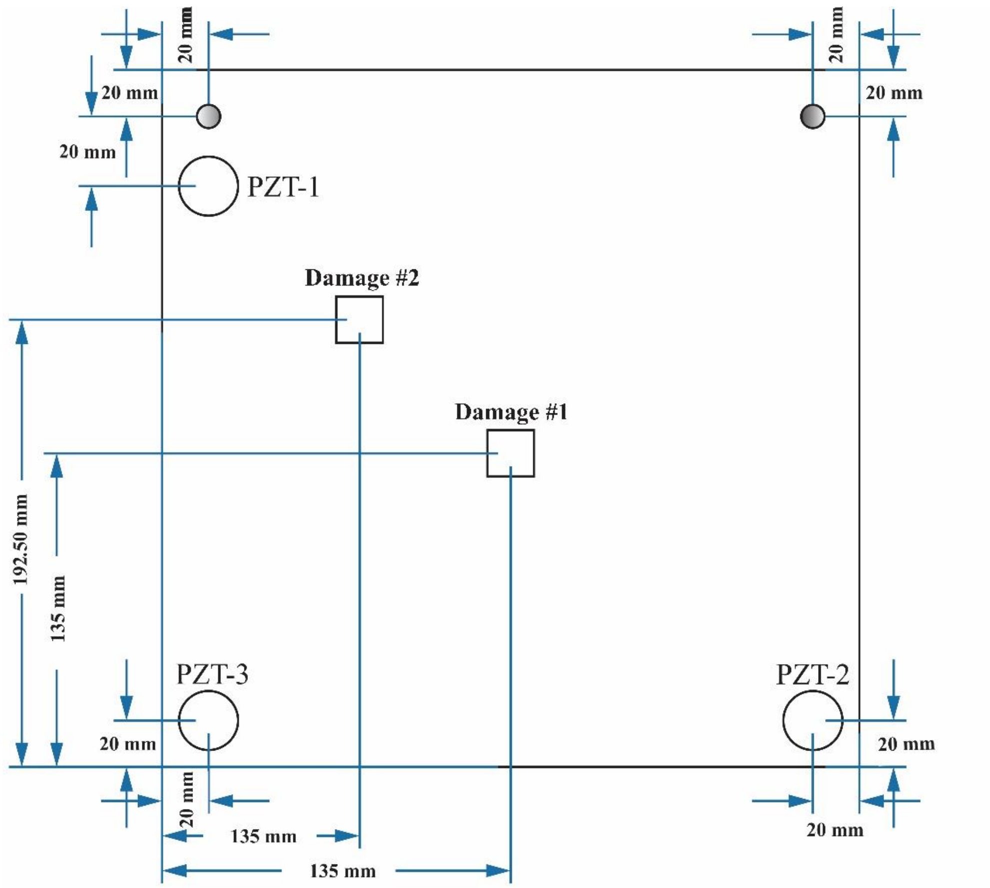

Figure 12: flowchart for B&K Precision Oscilloscope configuration.

The structure was hung vertically by thin fishing lines so that there was no greater interference from boundary conditions and the weight of the structure (holes 20 mm from the top edge). The type of virtual damage applied to the structure was by adding mass to the system in different positions. Thus, three cubic neodymium magnets (10 mm side) were mechanically coupled to the structure, two of them being coupled stacked on one side and the third on the opposite surface of the plate, in order to generate an increase in local stiffness in the two simulated positions.

The different positions used for the damage simulation aimed to visualize the potential of the Lamb Wave SHM method regarding the physical location of the damage. Thus, the position was defined with the objective of carrying out a process of triangulation of the position of the damage, contributing to the understanding of the results. The positions considered for the fault conditions can also be seen in Figure 12.

It should be noted that the weight of each magnet used is 2.1g, thus representing an increase in mass of about 1.24% compared to the total weight of the whole mechanical system. This configuration was adopted in order to verify the potential of the method in terms of identifying incipient damages.

In general, two inspection paths were adopted for the acquisition of Lamb Waves during the experiment, the PZT-1 patch was considered as an actuator in both cases and the other transducers were used as sensors in each particular path.

Then, the PZT-1 transducer was connected to the OUT-output terminal of the function generator and the other patch (PZT-2 and PZT-3) was connected to one of the channels of the 2530 B&K Precision digital oscilloscope. The connection of the transducers to the electronic equipment was made according to Figure 6.3, with the aid of probes.

The way of excitation of the PZT-1 actuator was based on a sweep of frequencies whose used range was 20-30kHz with a step of 33Hz. In all, 20 samples from each state were collected for each inspection path, thus totaling a population of 120 signal samples. Thus, 40 signatures were collected for a baseline: 20 samples PZT-1/PZT-2 and 20 samples PZT-1/PZT-3. Likewise, 40 signatures for damage 1 and 40 for damage 2.

After the acquisition step, CWT and DI algorithms were used in order to abstract the characteristics of the signals and later quantify the presence of damage in this structure. Such steps were applied in order to validate the acquisition system developed in this work.

Through the analysis of the Lamb Wave sets obtained by the experimental procedure, it was verified the need to apply an algorithm that allows the abstraction and separability of the states of the structure. This is because incipient or light damage promotes a very subtle variation in the vibration signature. Therefore, CWT was applied to the set of signals in order to extract the different characteristic frequency scales.

Figures 13 and 14 illustrate the average frequency scales obtained by applying the CWT in the different data sets, taking into account their respective inspection path.

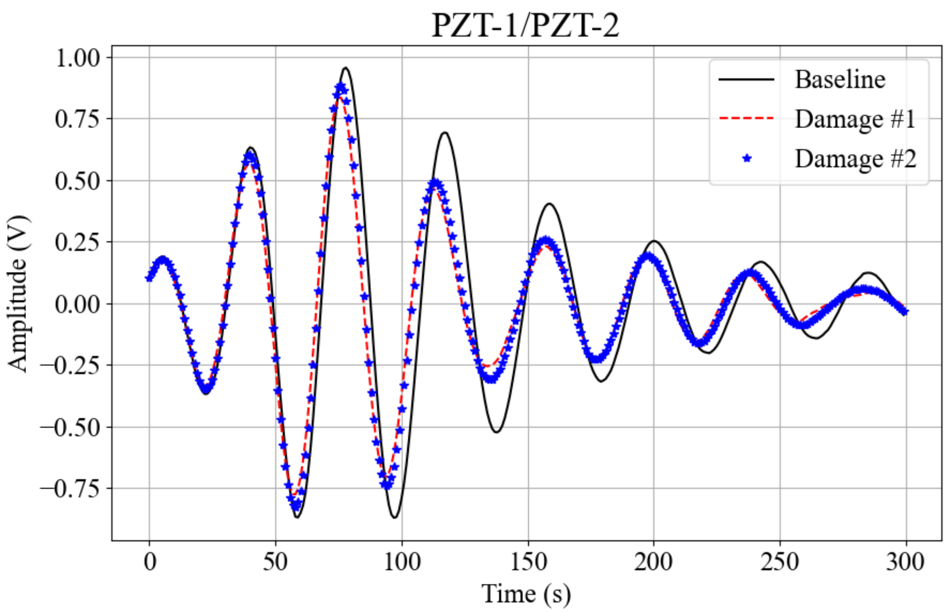

Figure 13: Averages of the characteristic wavelet scales of the states of the structure - Path PZT-1/PZT-2.

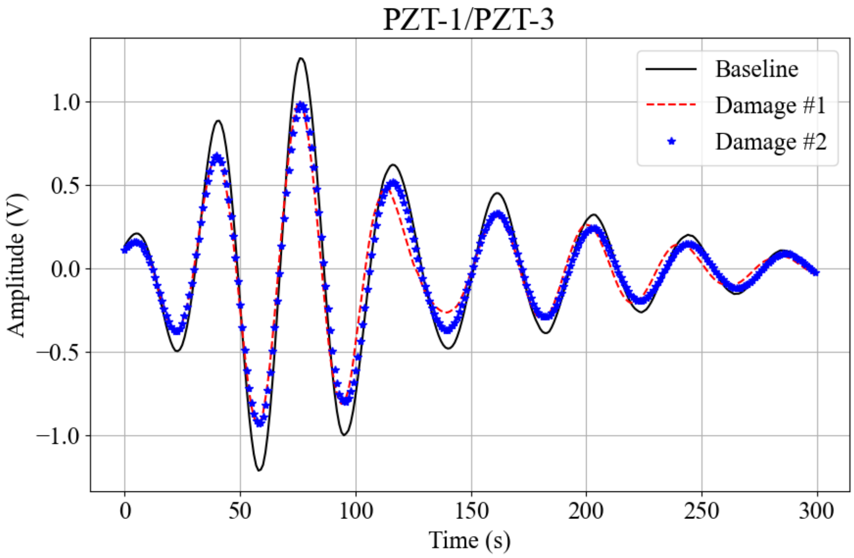

Figure 14: Averages of the characteristic wavelet scales of the states of the structure - Path PZT-1/PZT-3.

It can be seen that with the application of the CWT algorithm in the different data sets, it was possible to define the different state conditions of the structure, as well as the qualitative evaluation of the presence and severity of the damage.

However, the process of graphical analysis of the averages of the signals (performed previously) only allows the verification of the presence of damage and not its quantification and characterization in terms of severity. Therefore, an algorithm in Python was developed and applied, as a second evaluation step, of the Damage Index as a damage metric, as previously described. The DI metric values obtained as a result of the developed algorithm are presented in the box plots of Figure 15.

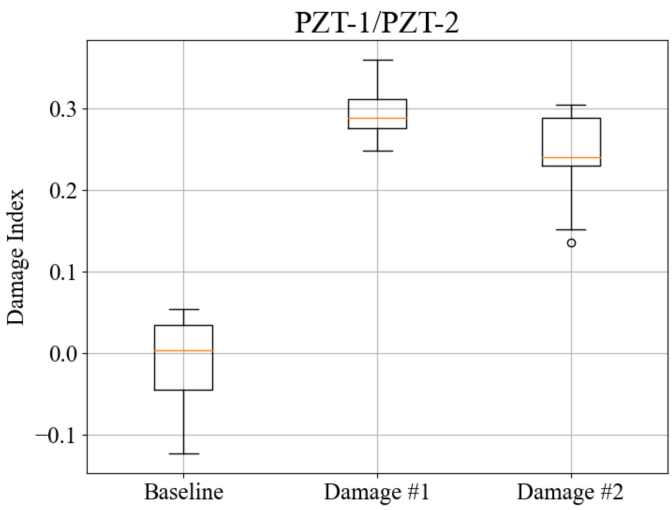

Figure 15: Boxplot of DI metric values for inspection path PZT-1/PZT-2.

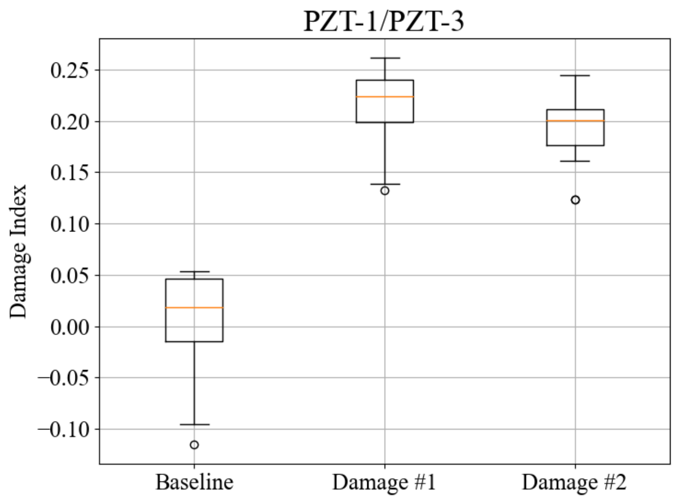

Figure 16: Boxplot of DI metric values for inspection path PZT-1/PZT-3.

From the boxplots shown in Figures 15 and 16, it can be seen that the proposed method was able to efficiently identify the presence of damage in the structure under study. Still, it can also be evaluated through the first graph that, although they are not linearly separable, the severity of Damage #1 is, in general, greater than that of Damage #2. This condition suggests that the location of this damage state is closer to the sensor than the Damage #2 state. Also, in an automatic system with a sensor network, it is possible to exploit this information through the inverse measures PZT-2/PZT-1.

The metric values obtained for the second inspection path (PZT-1/PZT-3) define that both damages are linearly equal or that their severity in relation to the inspection path is, reasonably, indifferent. This is due to the fact that the Lamb Waves are linearly influenced by the insertion mode, that is, their efficiency is more considerable in a perpendicular path between the actuator and the sensor.

Therefore, with this experiment, the applicability of the acquisition system can be evidenced, as well as the potential of the Lamb Wave SHM method in structural integrity analysis. However, it is necessary to remember that the applicability of the technique it depends on: an integrated sensor/actuator network, statistical or AI-based models for locating and quantifying the severity, and monitoring being focused on thin structures.

7.1. Final remarks – Brief State of the Art

This section presents a brief state of the art of acquisition systems used in the Structural Health Monitoring by Lamb Waves considering values in BRL in the year 2019. The currency presented is due to the high number of Brazilian colleagues who have acquired an interest in the technique.

At first, the literature describes several works that employ different fault acquisition systems by ultrasonic inspection. However, these systems usually have a high aggregate cost (over BRL 30,000) in addition to being robust compared to frequency domain acquisition systems (LEDESMA, 2015). Thus, although they have high precision, their characteristics make them a limiting factor regarding the use of these systems in-field analysis, as well as their use by schools with few financial resources. As a result, in order to develop practical and portable systems for integrity analysis by Lamb Waves, new instrumental configurations have been studied in recent decades (Farias et al., 2011; Asadi et al., 2017).

In this sense, Table 4 presents the recent instrumentation setups of the guided Lamb Waves inspection technique, linking them to their respective authors and the year of publication.

Table 4: Different authors and respective setups.

Setup	Authors	Cost
Wave Generator: PXI-5421 Module, Oscilloscope: PXI-5105 module, Signal Amplifier: Module A-303 A.A. Transducers: PZT (7.56 mm diameter per 1mm wide)	Keulen, Yildiz and Suleman (2014)	BRL 56,590
Wave Generator: PXI-5412 Module, Oscilloscope: PXI-5122 Module, Signal Amplifier: Falco WMA-320 Transducers: P-876 Patch DuraAct	Hettler et al. (2015)	BRL 60,302
Wave Generator: PXI-5412 Module, Oscilloscope: PXI-5105 Module, Transducers: PZT 5H (15 mm diameter per 0.5mm wide)	Rocha, Finzi Neto and Steffen Jr (2017)	BRL 43,415
PSV-400-3D-M Doppler Vibrometer	Soleimanpour (2016) Ji et al. (2018)	On-demand

In the work developed by Keulen, Yildiz and Suleman (2014), a network of PZT sensors was used to identify laminations in a carbon fiber-epoxy composite panel. For that, a PXI-5421 wave generator module and an A-303 A.A. signal amplifier were used in order to transmit Lamb Waves in the structure at a cutoff frequency of 265 kHz. Subsequently, the dynamic responses were collected on the PXI-5105 oscilloscope and a process of triangulation of the damaged region was performed using the RAPID (Reconstruction Algorithm for Probabilistic Inspection of Damage) tomographic reconstruction algorithm.

Hettler et al. (2015) used a system consisting of a PXI-5412 modular function generator and an NI PXI-5122 digital oscilloscope module to generate guided Lamb Waves on carbon fiber polymer (CFRP) reinforced plates. This function generator can generate standard waveforms (sine, triangle, square, and ramp) with bandwidths up to 20 MHz and amplitude ranging from -6V to 6V. The signals imposed on the actuator network were amplified through a WMA-320 laboratory amplifier and later captured through the sensor, both actuators and sensors are PVDF P-876 patches. Subsequently, a RAPID tomographic reconstruction algorithm was applied in order to obtain the parameters of location and extent of impact damage.

Rocha, Finzi Neto and Steffen Jr (2017) studied the influence of physical uncertainties (electronic components) of data acquisition systems, as well as environmental factors (temperature) on the integrity analysis procedure by Lamb Waves. For this, a 2024-T3 aluminum plate was instrumented in the pitch-catch configuration, that is, using two PZT transducers at different ends of the structure. A PXI-5412 function generator was used to apply a sine wave with a frequency of 30kHz and an amplitude of 10 Vpp. The dynamic response was measured with the PXI-5105 module with a sampling rate of 30MSa/s, with 30 thousand samples in total. It was observed that the temperature variation is a limiting factor for the damage inference process. Santos et al. (2016), observed the same relationship in the study of beams. Furthermore, it can be observed in the literature the use of this configuration in other works, such as (Moura Jr, 2008; Leucas, 2009).

Soleimanpour (2016) investigated the nonlinearity of Lamb Waves in composite beams. For this, experimental results were compared with the results obtained in a three-dimensional finite element model. The PSV-400-3D-M laser optical system was used to perform a triangulation of the surface modal nodes. This was possible through the variation of frequencies resulting from the lights of the three lasers that compose it. This configuration was replicated by Ji et al. (2018) for thin structures.

Still, alternative systems for inspection of structural integrity by Lamb Waves can be cited in the literature, which has lower cost instrumentation. The WSHM system developed by Ledesma (2015) uses transducers remotely controlled through a ZigBee network. However, there is greater complexity in using this system due to greater technical expertise in instrumentation.

7.2. References

Afshari, M. Vibration-and Impedance-based Structural Health Monitoring Applications and Thermal Effects. Ph.D. dissertation —Virginia Tech, 2012.

Asadi, S. et al. Implementation of a novel efficient low-cost method in structural health monitoring. *Smart Materials and Structures*, IOP Publishing, v. 26, n. 5, p. 055032, 2017.

Bailey, J. et al. Evidence relating to object-oriented software design: A survey. In: IEEE. null. [S.l.], 2007. p. 482–484.

Cardoso, L. B. et al. Estudo dos modos de propagação das ondas guiadas em estruturas cilindricas de aço carbono. In: *VII CONNEPI-Congresso Norte Nordeste de Pesquisa e Inovação*. [S.l.: s.n.], 2012.

Cardoso, L. F.; Silva, V. M.; Segundo, F. C. G. Osciloscópio de baixo custo utilizando a plataforma Arduino. *Anais do Encontro de Computação do Oeste Potiguar ECOP/UFERSA* (ISSN 2526-7574), v. 1, n. 1, 2017.

Chen, X.; Chen, J. Design of an arbitrary waveform signal generator. *Procedia Engineering*, Elsevier, v. 15, p. 2500–2504, 2011.

Cheraghi, N.; Taheri, F. A damage index for structural health monitoring based on the empirical mode decomposition. *Journal of Mechanics of Materials and Structures*, Mathematical Sciences Publishers, v. 2, n. 1, p. 43–61, 2007.

Cooper, I. D. What is a “mapping study?”. *Journal of the Medical Library Association: JMLA*, Medical Library Association, v. 104, n. 1, p. 76, 2016.

Corrêa, L. d. A. Estudo de propagação de ondas em tubos epóxi reforçado com fibra de vidro. 2014.

Cui, L.; Liu, Y.; Soh, C. K. Identification of crack size and orientation in continuous cylindrical structure using macro-fiber composite. *Journal of Intelligent Material Systems and Structures*, Sage Publications Sage UK: London, England, v. 25, n. 5, p. 596–605, 2014.

Dalton, R. P. The propagation of Lamb waves through metallic aircraft fuselage structure. Tese (Doutorado)—Department of Mechanical Engineering, Imperial College London 2000., 2000.

Debnath, L.; Shah, F. A. Wavelet transforms and their applications. [S.l.]: Springer, 2002.

Domingues, M. et al. Explorando a transformada wavelet contínua. Caderno Brasileiro de Ensino de Física, v. 38, n. 3, 2016.

Farias, C. et al. Estudo da propagação das ondas de Lamb em chapas de alumínio com furos de diferentes profundidades. In: *5th Pan American Conference For NDT*, COPAEND, Cancun, México. [S.l.: s.n.], 2011.

Franco, V. R. Monitoramento da integridade em estruturas aeronáuticas. Universidade Estadual Paulista (UNESP), 2009.

Fu, H.; Cohen, R. E. Polarization rotation mechanism for ultrahigh electromechanical response in single-crystal piezoelectrics. *Nature*, Nature Publishing Group, v. 403, n. 6767, p. 281, 2000.

Hettler, J. et al. Application of a probabilistic algorithm for ultrasonic guided wave imaging of carbon composites. *Physics Procedia*, Elsevier, v. 70, p. 664–667, 2015.

Islam, M.; Huang, H. Effects of adhesive thickness on the lamb wave pitch-catch signal using bonded piezoelectric wafer transducers. *Smart Materials and Structures*, IOP Publishing, v. 25, n. 8, p. 085014, 2016.

Ji, H. et al. Investigations on flexural wave propagation and attenuation in a modified one-dimensional acoustic black hole using a laser excitation technique. *Mechanical Systems and Signal Processing*, Elsevier, v. 104, p. 19–35, 2018.

Keulen, C. J.; Yildiz, M.; Suleman, A. Damage detection of composite plates by Lamb wave ultrasonic tomography with a sparse hexagonal network using damage progression trends. *Shock and Vibration*, Hindawi, v. 2014, 2014.

Kobayashi, M. et al. Structural health monitoring of composites using integrated and flexible piezoelectric ultrasonic transducers. *Journal of Intelligent Material Systems and Structures*, Sage Publications Sage UK: London, England, v. 20, n. 8, p. 969–977, 2009.

Kudela, P. et al. Structural health monitoring system based on a concept of Lamb wave focusing by the piezoelectric array. *Mechanical Systems and Signal Processing*, Elsevier, v. 108, p. 21–32, 2018.

Leão, R. J. et al. Simulação da propagação de ondas ultrassônicas longitudinais em materiais estruturais aeroespaciais. [sn], 2012.

Ledesma, N. E. C. Desenvolvimento de um sistema de SHM sem fio e com compensação automática de temperatura. PhD Dissertation – Universidade Estadual Paulista, 2015.

Leucas, L. d. F. Utilização das técnicas de Impedância eletromecânica e ondas de Lamb para identificação de dano em estruturas com rebites. Master Thesis – Universidade Federal de Uberlândia, 2009.

Lu, G. et al. Characterization of ultrasound energy diffusion due to small-size damage on an aluminum plate using piezoceramic transducers. *Sensors*, Multidisciplinary Digital Publishing Institute, v. 17, n. 12, p. 2796, 2017.

Mechbal, N.; Rebillat,M. Damage indexes comparison for the structural health monitoring of a stiffened composite plate. A. Güemes, A. Benjeddou, J. Rodellar and Jinsong Leng, 2017.

Mei, H.; Giurgiutiu, V. Effect of structural damping on the tuning between piezoelectric wafer active sensors and lamb waves. *Journal of Intelligent Material Systems and Structures*, SAGE Publications Sage UK: London, England, v. 29, n. 10, p. 2177–2191, 2018.

Moura Jr, J. d. R. V. Uma contribuição aos sistemas de monitoramento de integridade estrutural aplicada a estruturas aeronáuticas e espaciais. PhD Dissertation – Universidade Federal de Uberlândia, 2008.

Oliveira, A. E. T. d. Uso das ondas de Lamb e Scholte para caracterização de líquidos. Universidade Estadual Paulista (UNESP), 2015.

Overly, T. G.; Park, G.; Farrar, C. R. Development of signal processing tools and hardware for piezoelectric sensor diagnostic processes. In: International Society For Optics And Photonics. Sensor Systems and Networks: Phenomena, Technology, and Applications for NDE and Health Monitoring 2007. [S.l.], 2007. v. 6530, p. 653018.

Palmos, E. Modeling of Lamb waves and application to crack identification. [S.l.], 2009.

Park, H. W. et al. Time reversal active sensing for health monitoring of a composite plate. *Journal of Sound and Vibration*, Elsevier, v. 302, n. 1-2, p. 50–66, 2007.

Pohl, J. et al. Experimental and theoretical analysis of lamb wave generation by piezoceramic actuators for structural health monitoring. *Experimental Mechanics*, Springer, v. 52, n. 4, p. 429–438, 2012.

Possani, D. et al. Ondas ultrassônicas: teoria e aplicações industriais em ensaios não destrutivos. Revista Brasileira de Física Tecnológica Aplicada, v. 4, n. 1, 2017.

Qiao, P.; Fana,W. Lamb wave-based damage imaging method for damage detection of rectangular composite plates. *Structural Monitoring and Maintenance*, Techno-Press, v. 1, n. 4, p. 411–425, 2014.

Rocha, L.; Finzi Neto, R.; Steffen JR, V. SHM baseado em ondas de Lamb e métodos estatísticos para o limiar de detecção de dano aplicado a estruturas de aeronaves. 2017.

Rocha, L. A. d. A. Identificação de dano em estruturas utilizando uma metodologia que integra a técnica da impedância eletromecânica e ondas de Lamb. PhD Dissertation – Universidade Federal de Uberlândia, 2017.

Santos, J. G. d. F. et al. Monitoramento utilizando a técnica de ondas de Lamb para detecção de dano em estruturas metálicas. In: *XXXVII Iberian Latin American Congress on Computational Methods in Engineering*. [S.l.: s.n.], 2016. v. 2, n. 30, p. 46–54.

Santos, M. J. S. F. d. Ondas ultra-sonoras guiadas na caracterização e controlo não destrutivo de materiais. PhD Dissertation – Faculdade de Ciências e Tecnologia de Coimbra, Portugal, 2004.

Saravanan, T. J.; Gopalakrishnan, N.; Rao, N. P. Damage detection in structural element through propagating waves using radially weighted and factored rms. *Measurement*, Elsevier, v. 73, p. 520–538, 2015.

Shen, Y. Structural health monitoring using linear and nonlinear ultrasonic guided waves. 2014.

Soleimanpour, R. Damage detection of defects using linear and nonlinear guided waves. PhD Dissertation – University of Adelaide, Australia, 2016.

Soleimanpour, R.; NG, C.-T. Locating delaminations in laminated composite beams using nonlinear guided waves. Engineering Structures, Elsevier, v. 131, p. 207–219, 2017.

Sun, Z.; Zhang, L.; Rose, J. L. Flexural torsional guided wave mechanics and focusing in pipe. *Journal of Pressure Vessel Technology*, American Society of Mechanical Engineers, v. 127, n. 4, p. 471–478, 2005.

Tsuruta, K. M. et al. Monitoramento de integridade estrutural de materiais compostos sujeitos a impactos empregando a técnica da impedância eletromecânica. Master Thesis – Universidade Federal de Uberlândia, 2008.

Venugopal, V. P.; Wang, G. Modeling and analysis of lamb wave propagation in a beam under lead zirconate titanate actuation and sensing. Journal of Intelligent Material Systems and Structures, SAGE Publications Sage UK: London, England, v. 26, n. 13, p. 1679–1698, 2015.

Viana, D. D.; Formoso, C. T.; Kalsaas, B. T. Waste in construction: a systematic literature review on empirical studies. In: ID Tommelein & CL Pasquire, 20th Annual Conference of the International Group for Lean Construction. San Diego, USA. [S.l.: s.n.], 2012. p. 18–20.

Wang, W. et al. Experimental and numerical validation of guided wave phased arrays integrated within standard data acquisition systems for structural health monitoring. *Structural Control and Health Monitoring*, Wiley Online Library, v. 25, n. 6, p. e2171, 2018.

Yu, L. et al. Corrosion detection with piezoelectric wafer active sensors using pitch-catch waves and cross-time–frequency analysis. *Structural Health Monitoring*, Sage Publications Sage UK: London, England, v. 11, n. 1, p. 83–93, 2012.

Zhang, L. et al. Health monitoring of cuplok scaffold joint connection using piezoceramic transducers and time reversal method. *Smart Materials and Structures*, IOP Publishing, v. 25, n. 3, p. 035010, 2016.